Structural, electrical, magnetic, and thermal studies of Cr-doped $La_{0.7}Ca_{0.3}Mn_{1-x}Cr_xO_3$ $(0 \leq x \leq 1)$ manganites

Neeraj Kumar,[1] H. Kishan,[1] Ashok Rao,[2] and V. P. S. Awana[1,a)]
[1]*Superconductivity and Cryogenics Division, National Physical Laboratory (CSIR), Dr. K.S. Krishnan Marg, New Delhi-110012, India*
[2]*Department of Physics, Manipal Institute of Technology, Manipal University, Madav Nagar, Manipal 576104, India*

(Received 29 October 2009; accepted 29 January 2010; published online 21 April 2010)

We report detailed structural, electrical, magnetic, and specific heat studies on $La_{0.7}Ca_{0.3}Mn_{1-x}Cr_xO_3$ manganites. Rietveld analysis of fitted and observed x-ray diffraction patterns exhibited the single-phase nature of all the studied materials, which crystallize in *Pbnm* space group. Successive substitution of Cr at Mn-site in $La_{0.7}Ca_{0.3}Mn_{1-x}Cr_xO_3$ manganites increases the electrical resistivity and decreases the characteristic insulator-metal transition temperature (T_{IM}) of the parent compound along with a humplike feature for higher Cr-content ($x > 0.06$) samples. The hump structure basically signifies the onset of antiferromagnetic (AFM) interactions as inferred by both the magnetic and infrared (IR) spectroscopy studies. The systematic suppression of FM state results in a spin glass (SG)-like behavior. IR studies revealed that the vibration mode at 413 cm^{-1} being associated with internal bending of MnO_6 octahedra, becomes softer, indicating an increase in distortion and hence the possible SG behavior. The critical exponents (α, β, and γ) are calculated from the heat capacity (C_P) data near the T_{IM}/T_{FM}. The same exhibited variations of their values with doping. In particular, the value of β increases from 0.37(x=0.0) to 0.43(x=0.04), clearly indicating the coexistence of both long and short range magnetic orders, i.e., tendency toward SG state for Cr-doped samples. On the basis of present results, it is suggested that Cr dilutes double-exchange based FM and rather promotes the AFM based superexchange interactions via Cr^{3+}/Mn^{4+} ions. Substitution of Cr systematically destroys both the metallic state and long range FM order. © *2010 American Institute of Physics*. [doi:10.1063/1.3342462]

I. INTRODUCTION

Magnetoresistance (MR) is the relative change in the electrical resistivity of any material upon the application of magnetic field, defined as

$$MR = [(\rho_H - \rho_0)/(\rho_H)] \times 100.$$

This is one of the important parameters for magnetic data storage, magnetic sensors, and spintronic devices.[1] During the past decade, very high value of MR ($\sim 10^6$%) was reported in the perovskite manganites materials and is known as colossal magnetoresistance (CMR).[1,2] In the perovskite structure (ABO_3 type), A is generally trivalent rare-earth ion such as La^{3+}, Pr^{3+}, and Nd^{3+} or divalent alkali-earth ion such as Ca^{2+}, Sr^{2+}, Ba^{2+}, etc., whereas B is the manganese ion, which can also be replaced by other trivalent transition metal ions. The parent compounds such as $LaMnO_3$, $PrMnO_3$, etc., are antiferromagnetic (AFM) insulators.[1,2] However, with strategic substitution of divalent ions at A site, some of the Mn^{3+} ions ($3d^3, t^3_{2g}e_g^1$) convert into the Mn^{4+} ions ($3d^3, t^3_{2g}e_g^0$) resulting in fascinating physical phenomena such as paramagnetic (PM) insulator to ferromagnetic (FM) conductor or various mixed magnetic phases viz. canted AFM/spin glass (SG) coupled with charge/orbital ordered states in a particular doping range.[3] The conduction in manganites has been proposed on the basis of the double-exchange (DE) mechanism between Mn^{3+}/Mn^{4+} via oxygen along with the strong electron-phonon coupling.[4] In manganite materials, the CMR effect is observed near the insulator-metal (I-M) transition, which can be tuned by changing the chemical composition of the compound. Doping at the rare-earth site indirectly affects the conduction mechanism with its repercussion on bandwidth and bond angle between the manganese ions.[5] On the other hand doping at the manganese site directly affects the conduction mechanism and hence one can tailor the properties of perovskite manganites in more effective way. Therefore, doping at Mn-site with other elements is expected to provide some important clues concerning the conduction mechanism of CMR as well as possible enhancement/change in the MR of manganites materials. It was found that doping at Mn-site generally results in the decrease in the I-M transition temperature.[6,7] Maignan *et al.*[8] reported nearly invariant T_C (Curie temperature) values in Cr-doped $Sm_{0.56}Sr_{0.44}Mn_{1-x}$ Cr_xO_3 system. On the other hand, Raveau *et al.*[9] found that doping of Cr and Co induces an insulator-metal transition in the insulating AFM phase of $Pr_{0.5}Ca_{0.5}MnO_3$ (PCMO) without applying magnetic field. Similarly magnetic phase diagram of $Nd(Mn_{1-x}Cr_x)O_3$ have been proposed, in which for $x > 0.6$, there is a transition from A-type AFM state to the FM state.[10] However there are only few studies on the thermal properties of Cr-doped $La_{0.7}Ca_{0.3}MnO_3$ (LCMO) in FM state, where spin ordering has a crucial role. Thermal critical exponents and amplitudes

a)Author to whom correspondence should be addressed. FAX: 0091-11-45609310. Tel: 0091-11-45609210. Electronic mail: awana@mail.nplindia.ernet.in. URL: www.freewebs.com/vpsawana/.

near the metal insulator or magnetic phase transitions determine the type of ordering and the ensuing process.[11] Martin *et al.*[12] investigated the critical exponent of $La_{0.7}Sr_{0.3}MnO_3$ (LSMO) single crystal by neutron study. Taran *et al.*[13] studied thermal properties of the LCMO, PCMO, and LSMO and showed a correlation between transport and magnetic properties. There is a large contradiction in physical properties and thermal exponent values of CMR materials from sample to sample. The lack of data for complete phase diagram and the large variation in the physical property results of manganite materials motivated us to study the effect of Cr^{+3} ion doping in LCMO manganite at close intervals. In this paper we present transport, magnetic and thermal behavior of Cr-doped LCMO manganites. We conclude from our magnetic, IR, and thermal studies that Cr dilutes DE based FM of LCMO and rather promotes the AFM based superexchange (SE) interactions via Cr^{3+}/Mn^{4+} ions.

II. EXPERIMENTAL

Samples with nominal composition $La_{0.7}Ca_{0.3}Mn_{1-x}Cr_xO_3$ $(0 \le x \le 1)$ have been prepared by conventional solid state reaction method. Stoichiometric ratio of La_2O_3, $CaCO_3$, Cr_2O_3, and MnO_2 (all from Sigma Aldrich chemical Ltd. with 99.9% purity) were mixed thoroughly to get homogeneous powders that were calcined at 1250 °C for 24 h. Such calcined mixtures were then pressed into pellets and sintered in air at 1400 °C for 36 h. X-ray diffraction (XRD) patterns were recorded at RIGAKU MINI FLEX II with Cu Kα radiation (1.54 Å). Electrical resistivity as a function of temperature was measured by conventional four probe method and infrared (IR) spectra were recorded on Nicolet FTIR-5700 spectrometer. Magnetic measurements were carried out using superconducting quantum interference device magnetometer (Quantum Design, MPMS). The magnetization was measured under zero-field cooled (ZFC) and field cooled (FC) conditions with 0.01 T applied field. The heat capacity (C_P) measurements were carried out on physical property measurement system from Quantum Design.

III. RESULTS AND DISCUSSIONS

A. Crystal structure

Figure 1 exhibits the single phased x-ray patterns of $La_{0.7}Ca_{0.3}Mn_{1-x}Cr_xO_3$ $(0 \le x \le 1)$ series powders. Using Rietveld refinement we were able to index the XRD peaks with orthorhombic structure in the *Pbnm* space group. Table I provides the lattice parameters of $La_{0.7}Ca_{0.3}Mn_{1-x}Cr_xO_3$ $(0 \le x \le 1)$ series. A regular shift toward higher 2θ is observed with increasing Cr concentration indicating a decrease in volume. Decreases in lattice volume with the Cr doping can be attributed to the smaller ionic size of Cr^{+3} (0.62 Å) than that of Mn^{+3} ion (0.64 Å).[14]

B. Resistivity measurement

Figure 2 shows the electrical resistivity behavior of the $La_{0.7}Ca_{0.3}Mn_{1-x}Cr_xO_3$ $(0 \le x \le 1)$ series. An insulator-metal (I-M) transition is observed at 260 K for the pristine LCMO sample that shifts to low temperatures with Cr doping. With

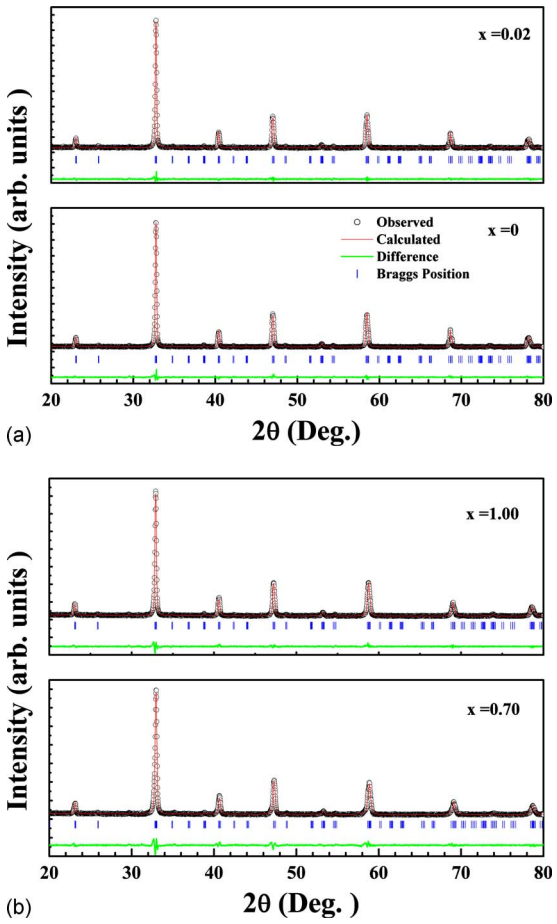

FIG. 1. (Color online) Reitveld fitted XRD patterns of $La_{0.7}Ca_{0.3}Mn_{1-x}Cr_xO_3$ $(x=0, 0.02, 0.70, 1.00)$.

increasing Cr-content an additional broad peak is also seen. For 20% Cr doping the high temperature I-M transition disappeared and only the broad peak is visible. For $x > 0.2$, all samples depict the insulating behavior. However at $x < 0.10$, Cr does not affect transition temperature faster.

These results can be understood in two ways; first the replacement of Mn^{3+} with Cr^{3+} can give rise to FM interaction via DE coupling as Cr^{3+} ion has same electronic structure $(3d^3, t^3_{2g}e_g^0)$ as Mn^{4+} and can be connected to Mn^{3+} ion

TABLE I. Unit-cell parameters and reliability factor (χ^2) for the refinements of $La_{0.7}Ca_{0.3}Mn_{1-x}Cr_xO_3$ $(0 \le x \le 1)$ phases in *Pbnm* space group.

$(L_{0.7}C_{0.3}M_{1-x}Cr_xO_3)$	a (Å)	b (Å)	c (Å)	χ^2	Volume (Å^3)
x=0.00	5.462	5.478	7.720	1.44	230.959
x=0.02	5.462	5.478	7.719	2.29	230.950
x=0.04	5.460	5.476	7.718	2.44	230.749
x=0.06	5.459	5.476	7.717	2.33	230.683
x=0.08	5.459	5.475	7.716	2.26	230.612
x=0.10	5.457	5.475	7.714	2.37	230.484
x=0.20	5.452	5.472	7.709	2.32	229.977
x=0.30	5.443	5.467	7.701	2.64	229.302
x=0.40	5.438	5.460	7.691	3.27	228.378
x=0.50	5.432	5.459	7.683	4.13	227.846
x=0.70	5.427	5.454	7.676	4.00	227.211
x=1.00	5.436	5.455	7.686	2.84	227.927

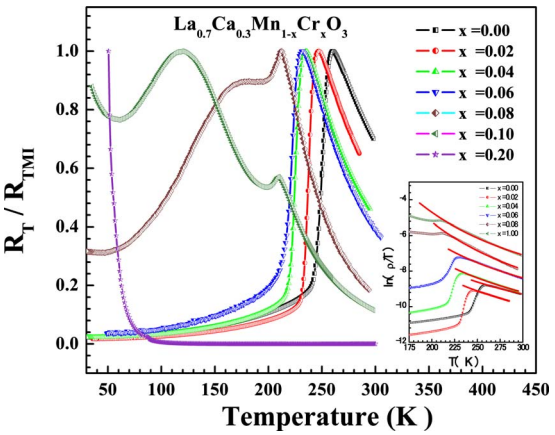

FIG. 2. (Color online) Electrical resistivity variation with temperature of the $La_{0.7}Ca_{0.3}Mn_{1-x}Cr_xO_3$ $(0 \leq x \leq 0.2)$ series.

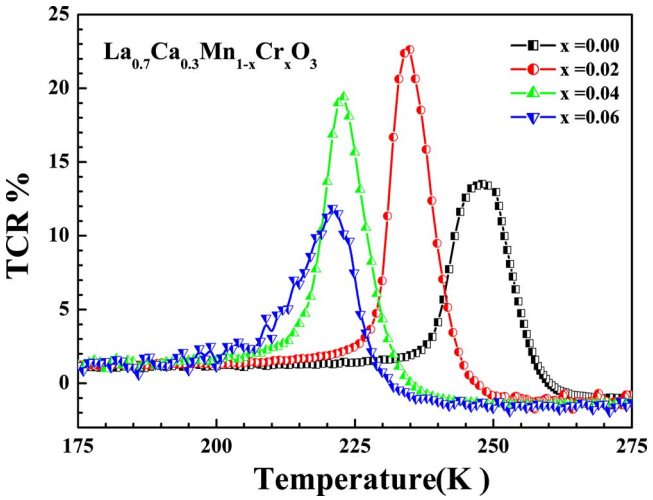

FIG. 3. (Color online) Temperature coefficient of resistance variation for the series $La_{0.7}Ca_{0.3}Mn_{1-x}Cr_xO_3$ $(0 \leq x \leq 0.06)$.

via oxygen in a similar way as for Mn^{4+}. Therefore, the DE interaction between Mn^{3+}/Cr^{3+} and Mn^{3+}/Mn^{4+} pairs may be thought responsible for the high temperature peak and a small sensitivity about transition temperature in the Cr-doped samples. The second peak may result from the AFM interaction due to SE mechanisms between Cr^{3+}/Cr^{3+} and/or Cr^{3+}/Mn^{4+} ions. There seems to be a competition between DE and SE mechanisms in these compounds. Second at low doping $(x \leq 0.10)$, as the Cr^{3+} ion environment mainly consists of Mn^{3+} ions, the ratio of Mn^{3+} and Mn^{4+} ions is not much affected. Whereas, at higher doping concentrations, there is an absolute reduction in Mn^{3+} ion in comparison with both Cr^{3+} and Mn^{4+} ions. This increases AFM correlations between Cr^{3+}/Mn^{4+} and Cr^{3+}/Cr^{3+} via SE interactions.

To further clarify this conjecture we analyzed the conduction mechanisms above T_{IM}. Above this temperature we fitted resistivity results by small range polaron model,

$$\rho = \rho_0 T \exp(E_\rho / k_B T), \quad (1)$$

where ρ_0 is a constant, E_ρ is the polaron activation energy, and k_B is the Boltzmann constant.[15,16] This model fits well in the insulating region except near T_{IM} (inset of Fig. 2). The fitting parameter reveals that the activation energy E_ρ increases (Table II) with increasing Cr doping. It is well known that polarons may arise due to strong lattice-electron interactions originated by the Jahn-Teller distortion.[5] This makes a strong correlation between activation energy and lattice distortion. It is reasonably accepted that with smaller Cr ion doping, distortion may tend to localize the carriers, hence lattice constant and activation energy have similar variation. Also as mentioned earlier, with an increase in doping of Cr some of Mn^{+4} ions are replaced by Cr^{+3} and probability of hopping of electrons from Mn^{+3} to Mn^{+4} may become difficult, resulting in an increase in the activation energy. Besides the lattice distortion effect due to Mn^{3+}/Cr^{3+} substitution, the DE interaction between Mn^{+3}/Cr^{+3} and Mn^{+3}/Mn^{+4} pairs may not be similar in nature and hence affecting the conduction process.

TABLE II. Activation energy calculations from the high temperature insulating region above T_{IM} using Eq. (1) and magnetic moment calculations using Eq. (2).

Composition $(L_{0.7}C_{0.3}M_{1-x}Cr_xO_3)$	Activation energy (meV)	T_{IM} (K)	$M(\mu_B)$ experimental	$M(\mu_B)$ calculated
x=0.00	88.037	260	3.96	3.7
x=0.02	97.954	247	⋯	⋯
x=0.04	103.997	235	⋯	⋯
x=0.06	112.124	231	⋯	⋯
x=0.08	117.735	212	⋯	⋯
x=0.10	123.501	210	3.59	3.18
x=0.20	⋯	⋯	2.64	2.66
x=0.30	⋯	⋯	1.88	2.14
x=0.40	⋯	⋯	1.43	1.62
x=0.50	⋯	⋯	0.80	1.1

Figure 3 reveals temperature coefficient of resistance (TCR) [TCR calculated as (1/R) (dR/dT)] values for samples $La_{0.7}Ca_{0.3}Mn_{1-x}Cr_xO_3$ $(0 \leq x \leq 0.06)$. For the parent compound TCR is 13.57%, however, it becomes nearly double (22.78%) for x=0.02, and further decreases with increasing the Cr concentration. Such high TCR can have large potential application as IR bolometers near the transition temperature. Interestingly though the T_{IM} is decreased with increased resistivity indicating relatively more localization effects, the TCR, i.e., measure of sharpness of the transition is improved in small Cr concentration regime. This could be attributed to ensuing morphological effects in terms of grain size, etc., instead of pure electronic process as discussed above.[17]

C. IR measurement

The electrical resistivity results are further corroborated by the IR spectroscopic measurements. The ideal cubic perovskite ABO_3 with space group O^1_h has 15 normal modes of vibration, in which only three are IR active mode in range of 200–800 cm^{-1}.[18] Any deviations from ideal cubic structure may cause change in vibration mode or IR spectra. IR spectra of $La_{0.7}Ca_{0.3}Mn_{1-x}Cr_xO_3$ $(x=0.0,0.1,0.3,0.5,0.7,1.0)$ are observed in the 400–750 cm^{-1} region and is shown in Fig. 4. The band due to in-phase stretching mode (B_{2g} mode) of oxygen is observed at 590 cm^{-1} for pristine compound that shifts to higher wave number (higher frequency) 631 cm^{-1} as concentration of Cr increases. The band at

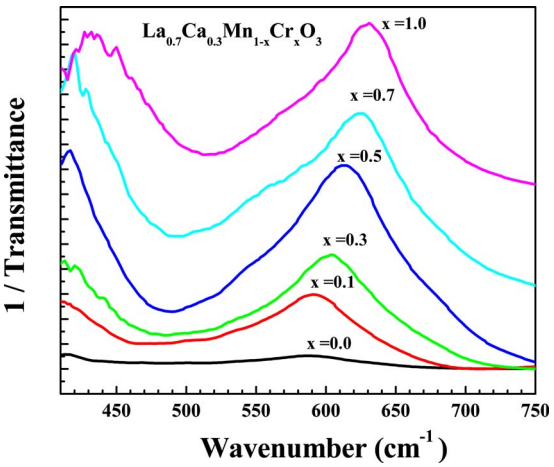

FIG. 4. (Color online) IR spectra for the series $La_{0.7}Ca_{0.3}Mn_{1-x}Cr_xO_3$ (x =0.0, 0.1, 0.3, 0.5, 0.7, 1.0).

413 cm^{-1} that is an E_g symmetry mode associated with an internal bending mode of MnO_6 octahedra becomes softer and new additional secondary vibration bands are generated. As ionic charge on both Mn^{3+} and Cr^{3+} is the same, the geometrical/lattice effect might be mainly responsible for the change in spectra. The increase in B–O vibration frequency from 590 to 631 cm^{-1} indicates strong coupling constant and hence the shorter bond lengths/decrease in lattice volume, supporting the XRD results.

Analyzing IR spectra one can conclude about the distribution of Mn^{3+} and Cr^{3+} ions. A symmetric band is expected if the Mn^{3+} and Cr^{3+} ions are distributed uniformly; if distribution is nonuniform then the band is expected nonsymmetric. For all Cr concentration a broad shoulder appears at lower wave number side implying that all the samples have more character of $La_{0.7}Ca_{0.3}CrO_3$ with minor character LCMO. The appearance of nonsymmetric bands and the shoulder at lower frequency side with increasing Cr concentration indicate the uneven distribution of Mn^{3+} and Cr^{3+} ions. For $La_{0.7}Ca_{0.3}Mn_{0.5}Cr_{0.5}O_3$ the band is observed at 612.5 cm^{-1}. This composition also has a broad shoulder toward lower wave number side, indicating the presence of pocketed $La_{0.7}Ca_{0.3}CrO_3$ and LCMO. Other possibility in the increase in the electrical resistivity may be due to strong coupling between orbital and the spin degrees of freedom (magnetic polarons) that localize the carriers. The FM (AFM) clusters can shrink (increase) with increasing Cr concentration. Metallic character gets suppressed through the percolation mechanism that is induced by Cr ions encouraging antiferromagnetism.[19] This is particularly effective for higher Cr concentration ($x > 0.20$) samples.

D. Magnetic measurement

To ascertain the presence of magnetic polarons we carried out magnetic measurements on some of the samples (Figs. 5 and 6). Like electrical resistivity behavior, parent compound (LCMO) shows a PM to FM transition with Curie temperature (T_C) ~255 K near the peak in electrical resistivity (~260 K). Below the transition temperature a pure FM phase is observed. Separation in M_{ZFC} and M_{FC} data indicates the magnetic inhomogeneity in long range FM ordering, which is also clear from the M-H plots taken at 5 and 100 K shown in Fig. 6.[20] With an increase in Cr doping other magnetic states such as mixed FM and AFM are observed. The coexistence of FM and AFM states is supported by M-T and M-H curves. The long range FM order is diluted even when a small amount of Cr is doped. For 10% Cr doping the ZFC and FC curves are very well bifurcated at low temperatures and there is a sudden drop in magnetic moment at around 40 K. This sudden drop represents some sort of magnetic anisotropy or magnetic frustration in the sample. Also from M-H curves it can be seen that the magnetization is not saturated even up to 10 kOe field and thus supports canted AFM state. It was recently reported by Capogna *et al.* that for 15% Cr doping the saturation does not occur even at 3 T. Further it was proposed that the canted AFM state arises due to random distribution of Cr^{3+} ions with random oriented spin[21] in Cr-doped systems. On increasing the Cr concentration this drop becomes sharper with a decrease in magnetic moment. With an increase in Cr doping, the SE driven AFM interactions become more prominent than the DE based FM. The AFM-FM phase transition is seen clearly for Cr=0.50.

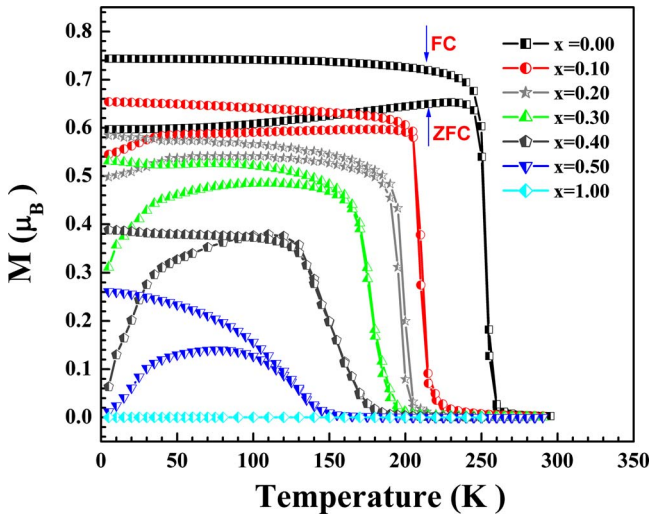

FIG. 5. (Color online) Magnetization variation with temperature of the $La_{0.7}Ca_{0.3}Mn_{1-x}Cr_xO_3$ ($0 \le x \le 1.0$) Series.

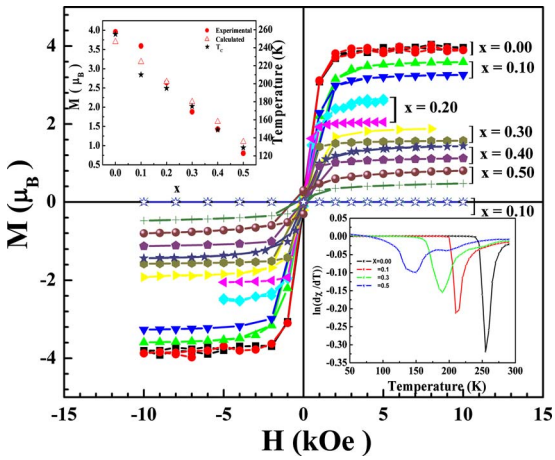

FIG. 6. (Color online) Magnetization variation with applied field of the $La_{0.7}Ca_{0.3}Mn_{1-x}Cr_xO_3$ ($0 \le x \le 1.0$) series taken at 5 and 100 K. The inset shows variation in magnetic moment with doping concentration (upper) and variation of $d(\ln \chi)/dT$ with temperature (lower).

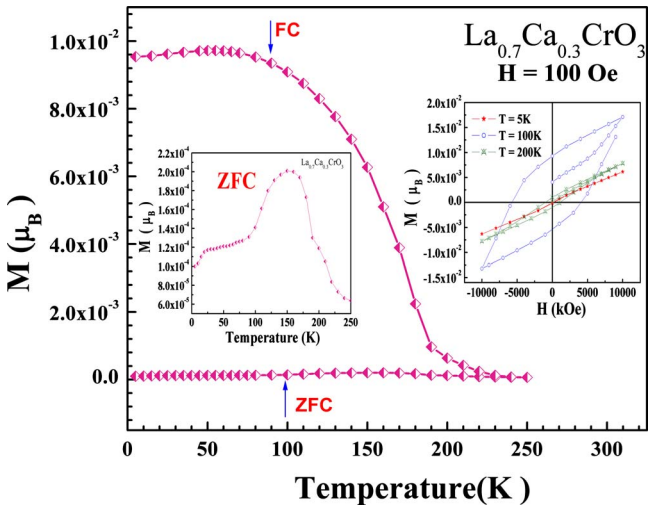

FIG. 7. (Color online) Magnetization variation in $La_{0.7}Ca_{0.3}CrO_3$. The inset shows the variation of Magnetization with temperature under zero-field condition (left) and magnetization variation with applied field taken at 5, 100, and 200 K (right).

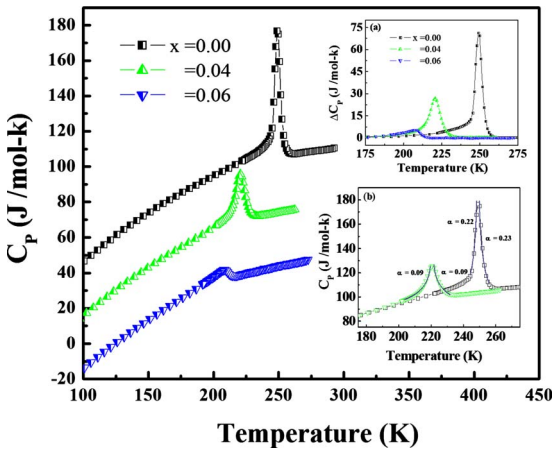

FIG. 8. (Color online) Temperature dependence of specific heat of $La_{0.7}Ca_{0.3}Mn_{1-x}Cr_xO_3$ (x=0, 0.04, and 0.06). The upper inset (a) shows the temperature dependence anomalous part of total specific heat and lower inset (b) shows the fitting curves based on fluctuation theory.

Though still there is canted spin state behavior generated by the competition between FM and AFM. Other indication can be found from the multiple peaks observed in $d(\ln \chi)/dT$ curves shown in the inset of Fig. 6. For the parent compound there is a single peak but with Cr concentration, an addition peak appears toward higher temperature. On complete replacement of Mn by Cr, only the strong AFM state with a little canting is present (Fig. 7). The magnetic moment drops more rapidly with an increase in Cr concentration. We tried to make a rough estimation for the prediction of magnetic moment of our system at 5 K. The chemical compound with the chemical formula $La^{3+}{}_{0.7}Ca^{2+}{}_{0.3}(Mn_{1-x}Cr_x)^{3+}{}_{0.7}(Mn_{1-x}Cr_x)^{4+}{}_{0.3}O_3$ leads to a magnetic moment of

$$M(\mu_s) = [4(0.7 - 0.7x) - 3(0.7x) + 3(0.3 - 0.3x) + 2(0.3x)]\mu_B = (3.7 - 5.2x)\mu_B. \quad (2)$$

Mn^{3+}, Mn^{4+}, Cr^{3+}, and Cr^{4+} ions have magnetic moments $\sim 4\mu_B$, $3\mu_B$, $3\mu_B$, and $2\mu_B$ respectively. The calculated and experimental values of magnetic moment per formula unit are listed in Table II and there variation with Cr concentration is shown in inset of Fig. 6. There is a small discrepancy in them. For the parent compound calculated magnetic moment is $3.96\mu_B$, which is about 6% more than the calculated value. This may be attributed to oxygen deficiency due to which there may be a small change in Mn^{3+} ion concentration.[22,23] This inhomogeneity is also supported by a small separation between FC and ZFC magnetization data. An increase in number of Mn^{3+} ion results in an increase in the magnetic moment. The agreement between experimental and calculated values of the magnetic moment guarantees the near full oxygen stoichiometry of the studies samples. For higher doping (Cr>0.5) this assumption is not valid because the system moves toward the competing FM to AFM states with ensuing SG behavior, and hence much less observed moments. The series end compound is AFM as shown in Fig. 7.

In summary, from magnetization data it is observed that Cr doping dilutes long range order of ferromagnetism. The SE interactions between Cr^{3+}/Mn^{4+} and Cr^{3+}/Cr^{3+} give rise to AFM ordering. The competing FM and AFM states may give rise to possible SG type behavior in the Cr-doped LCMO.

E. Specific heat

The temperature dependence specific heat is shown in Fig. 8. For the sake of clarity each data has been shifted by 30 J/mol K with respect to parent LCMO sample. With increasing Cr concentration, the transition temperature (T_{cp}) decreases. Even with x=0.06 the transition temperature drops to 208 from 249 K for the parent compound. The relative change in transition temperature is only about 16% in comparison with Mn-site Ti doping that changes the T_{cp} by 50% in LCMO system.[24] Relatively less sensitivity of Cr doping toward T_{cp} in comparison with Ti indicates the possibility of some Cr being involved in DE mechanism.[25] Anomalous part of specific heat (ΔC_p) related to the peak at transition temperature was extracted by subtracting background from the total specific heat (see the upper inset of Fig. 8). To approximate our data for the specific heat, we first calculated entropy change (ΔS) near the transition temperature by integrating $\Delta C_p/T$ versus T curves, which is found to decreases with increasing Cr concentration. The calculated values of ΔS are 0.36R, 0.21R, and 0.06R for x=0.0, 0.04, and 0.06, respectively, where R is the gas constant. The theoretical value for the parent compound is about R ln 2, which is nearly double the experimental value. The results for the parent compound suggest some sort of inhomogeneity or partial canted spin in the FM state.[26] This situation is abundant in most of polycrystalline LCMO.[27] With Cr substitution the observed entropy change (ΔS) near the transition temperature decreases sharply and only a small fraction of the theoretical entropy is observed. This can be understood in terms of fast suppression of DE driven long range FM order being diluted by increasing SE driven AFM with short SG correlations resulting in less net entropy with progressive Cr doping.

Further to investigate the behavior around the transition temperature, we use the expression from fluctuation theory of phase transition,[28]

$$C_p = A \times t^{-\alpha}, \quad (3)$$

where $t=1-(T/T_c)$ for $T<T_{cp}$ and $t=(T/T_c)-1$ for $T>T_{cp}$, defined as the reduced temperatures. α is the critical exponent of specific heat and A is related to the critical amplitude. Calculated value of critical exponent and ratio of critical amplitude below and above the T_{cp} are 0.22, 0.23, and 1.04 for x=0.0 and 0.09, 0.09 and 0.99 for x=0.04, see fitting of the experimental data in lower inset of Fig. 8. Interestingly, the x=0.06 deviates from the theoretical fluctuation theory. Similarly for critical exponent β at $T<T_{cp}$, we follow

$$C_p = B \times t^{2\beta-1}(T_c/T)^2. \quad (4)$$

Here B is a constant and β describes spin behavior in the FM state.[29] The calculated values of critical exponent β are 0.38 and 0.43 for x=0.0 and 0.04 samples, respectively, which lies between theoretical mean-field model (β=0.5) and the Heisenberg and Ising model (β=0.37).[30] For parent compound β lies near the Ising model and Heisenberg model supports the presence of DE. On the other hand with x=0.04 critical exponent seems to move toward mean-field theory value that supports the coexistence of both long- and short-range magnetic orderings simultaneously. Also we calculated the critical exponent γ that links the spontaneous magnetization (M) and inverse magnetic susceptibility (χ^{-1}) above the Curie temperature, i.e., $\chi^{-1}=B[(T/T_c)-1]^{-\gamma}$,[30] where B is the critical amplitude. Using scaling law,

$$\alpha + 2\beta + \gamma = 2. \quad (5)$$

The values are found to be 1.01 and 1.05 for x=0.0 and 0.04 samples, respectively. γ values are nearer to mean-field model and a slight increase in value supports that with Cr doping the magnetic inhomogeneity increase.

In a nutshell with Cr doping, net entropy decreases along with critical exponent's β and γ increases. Decrease in net entropy indicates toward the suppression of long range magnetic order with Cr doping. For parent compound β lies near the Heisenberg model. On the other hand with x=0.04 the same moves toward mean-field theory, supporting the coexistence of both long- and short-range magnetic orderings in the Cr-doped samples.

IV. CONCLUSIONS

We have investigated the effect of Cr doping on structural, electrical, magnetic, and thermal properties of LCMO. By the Rietveld refinement of the x-ray data, it is observed that Cr could replace Mn completely. The insulator-metal transition temperature decreases with Cr doping. At lower concentration of Cr, DE between Mn^{3+} and Mn^{4+} ions is not affected and Cr seems to take part in DE supported by resistivity and specific heat measurements. Both critical exponents β and γ increase and move toward the mean-field theory. At higher concentration AFM interaction originates from SE between Cr^{3+}/Mn^{4+} and Cr^{3+}/Cr^{3+} with reflection as an additional broad peak in the electrical resistivity. The magnetic measurements also corroborate the presence of competing FM and AFM interactions in the doped system.

ACKNOWLEDGMENTS

The authors acknowledge keen interest and encouragement provided by Professor R. C. Budhani, Director-NPL. N.K. further acknowledges the financial support from the CSIR in terms of the CSIR-SRF Fellowship to carry out research work at NPL and pursue for his Ph.D. thesis.

[1] C. N. R. Rao and B. Raveau, *Colossal Magnetoresistance Charge Ordering and Related Properties of Manganese Oxide* (World Scientific, Singapore, 1998).
[2] A. M. Haghiri-Gosnet and J. P. Renard, J. Phys. D: Appl. Phys. **36**, R127 (2003).
[3] Y. Tokura, Rep. Prog. Phys. **69**, 797 (2006).
[4] C. Zener, Phys. Rev. **82**, 403 (1951).
[5] A. J. Millis, Nature (London) **392**, 147 (1998).
[6] D. N. H. Nam, N. V. Dai, T. D. Tanh, L. T. C. Tuong, L. V. Hong, and N. X. Phuc, Phys. Rev. B **77**, 224420 (2008).
[7] S. K. Agarwal, N. Panwar, V. Sen, and D. K. Panya, J. Phys. D: Appl. Phys. **41**, 105004 (2008).
[8] A. Maignan, F. Damay, A. Barnabe´, C. Martin, M. Hervieu, and B. Raveau, Philos. Trans. R. Soc. London, Ser. B **356**, 1635 (1998).
[9] B. Raveau, A. Maignan, and C. Martin, J. Solid State Chem. **130**, 162 (1997).
[10] Zh. Yang, L. Ye, and X. Xie, J. Phys.: Condens. Matter **12**, 2737 (2000).
[11] H. E. Stanley, *Introduction to Phase Transition and Critical Phenomena* (Clarendon, Oxford, 1971); *Introduction to Phase Transition and Critical Phenomena* (Mir, Moscow, 1973).
[12] M. C. Martin, G. Shirane, Y. Endoh, K. Hirota, Y. Moritomo, and Y. Tokura, Phys. Rev. B **53**, 14285 (1996).
[13] S. Taran, B. K. Chaudhuri, S. Chatterjee, H. D. Yang, S. Neeleshwar, and Y. Y. Chen, J. Appl. Phys. **98**, 103903 (2005).
[14] R. D. Shannon, Acta Crystallogr., Sect. A: Cryst. Phys., Diffr., Theor. Gen. Crystallogr. **32**, 751 (1976).
[15] A. S. Alexandrov and B. Ya. Yavidov, Phys. Rev. B **69**, 073101 (2004).
[16] N. F. Mott and E. A. Davis, *Electronic Processes in Non-Crystalline Materials* (Clarendon, Oxford, 1979).
[17] V. P. S. Awana, R. Tripathi, S. Balamurugan, H. Kishan, and E. Takayama-Muromachi, Solid State Commun. **140**, 410 (2006).
[18] A. Tkachuk, K. Rogachi, D. E. Brown, B. Dabrowski, A. J. Fedro, C. W. Kimball, B. Pyles, X. Xiong, D. Rosenmann, and B. D. Dunlap, Phys. Rev. B **57**, 8509 (1998).
[19] M. Uehara, S. Mori, C. H. Chen, and S. W. Cheong, Nature (London) **399**, 560 (1999).
[20] C. S. Hong, E. O. Chi, W. S. Kim, N. H. Hur, K. W. Lee, and C. H. Lee, Chem. Mater. **13**, 945 (2001).
[21] L. Capogna, A. Martinelli, M. G. Francesconi, P. G. Radaelli, R. Carvajal, O. Cabeza, M. Ferretti, C. Castellano, T. Corridoni, and N. Pompeo, Phys. Rev. B **77**, 104438 (2008).
[22] J. M. D. Coey, M. Viert, and S. Von Molnar, Adv. Phys. **48**, 167 (1999).
[23] O. F. de Lima, J. A. H. Coaquira, R. L. de Almeida, L. B. de Carvalho, and S. K. Malik, J. Appl. Phys. **105**, 013907 (2009).
[24] R. W. Li, Z. H. Wang, X. Chen, J. R. Sun, B. G. Shen, and C. H. Yan, J. Appl. Phys. **87**, 5597 (2000).
[25] D. C. Kundaliya, R. Vij, R.G. Kulkarni, B. Varughese, A. K. Nigan, and S. K. Malik, J. Appl. Phys. **98**, 013905 (2005).
[26] L. M. Wang, J.-H. Lai, J.-L. Wu, Y.-K. Kuo, and C. L. Chang, J. Appl. Phys. **102**, 023915 (2007).
[27] V. P. S. Awana, E. Schmidt, E. Gmelin, A. Gupta, A. Sedky, A. V. Narlikar, C. A. Cardoso, O. F. de Lima, S. K. Malik, and W. B. Yelon, J. Appl. Phys. **87**, 5034 (2000).
[28] A. K. Murtazaev, S. B. Abdulvagidov, and A. M. Aliev, Phys. Solid State **43**, 1103 (2001).
[29] D. Kim, B. L. Zink, F. Hellman, and J. M. D. Coey, Phys. Rev. B **65**, 214424 (2002).
[30] J. Alonso, L. A. Fernanadez, F. Guinea, V. Laliena, and V. Martin-Mayor, Nucl. Phys. B **596**, 587 (2001).